ARTICLE

Plasticity of the Human Visual System in Response to Retinal Gene Therapy in a Group of Patients with Leber's Congenital Amaurosis

Manzar Ashtari[1,2†], Hui Zhang[3], Philip A. Cook[4], Laura L. Cyckowski[5], Kenneth S. Shindler[6, 2], Kathleen A. Marshall[1,7], Puya Aravand[2, 6], Arastoo Vossough[5], James C. Gee[4], Albert M. Maguire[1, 2,6], Chris I. Baker[8], Jean Bennett[1, 2,6]

[1] Department of Ophthalmology, Children's Hospital of Philadelphia, Philadelphia, PA 19014, USA. [2] Center for Advanced Retinal and Ocular Therapeutics, University of Pennsylvania Perelman School of Medicine, 309 Stellar-Chance Labs, 422 Curie Blvd, Philadelphia, PA 19104; [3] Department of Computer Science, University College London. Gower Street, London WC1E 6BT, United Kingdom. [4] Penn Image Computing and Science Lab, Department of Radiology, University of Pennsylvania, 3600 Market Street, Philadelphia, PA 19104, USA. [5] Department of Radiology, The Children's Hospital of Philadelphia, Philadelphia, PA 19014, USA. [6] F. M. Kirby Center for Molecular Ophthalmology, Scheie Eye Institute, University of Pennsylvania, 309 Stellar-Chance Labs, 422 Curie Boulevard, Philadelphia, PA 19104, USA. [7] Center for Cellular and Molecular Therapeutics at The Children's Hospital of Philadelphia, Colket Translational Research Building, 3501 Civic Center Boulevard, Philadelphia, PA 19014, USA. [8] Laboratory of Brain and Cognition, National Institute of Health, 10 Center Drive, MSC 1240, Bethesda, MD 20892, USA
†To whom correspondence should be addressed: E-mail: ashtari@chop.edu

Abstract

Much of our knowledge of the mechanisms underlying plasticity in the visual cortex in response to visual impairment, vision restoration, and environmental interactions, stems from animal studies. Here, we evaluate human brain plasticity *in vivo,* in a group of patients who regained vision through gene therapy. Using noninvasive multimodal neuroimaging methods we demonstrate that reversing blindness through gene therapy promotes long-term structural plasticity. Results show significant normalization along the visual pathway corresponding to the site of retinal injection compared with projections from untreated retina. Results indicate significant improvement along the visual pathway corresponding to the site of retinal injection compared with projections from untreated retina. After gene therapy, treated visual pathways were not different from those in control subjects, while untreated projections deteriorated. Our

results suggest that visual experience, enhanced by gene therapy, may be responsible for the reorganization and maturation of synaptic connectivity of the treated visual pathways. This joint collaboration and interaction between the eye and brain enables improved and sustained long-term visual function.

Introduction

Much of our knowledge of plasticity in the human visual system comes from studies investigating the impact of sensory input deprivation. For example, studies of blind individuals have suggested recruitment of the visual cortex for non-visual tasks such as Braille reading(*4*) or even verbal memory(*5*). However, there are limited studies regarding the effects on plasticity following the enhancement of visual input (primarily single case studies)(*6*, *7*). Here, we evaluate plasticity following the restoration of visual function in a group of subjects who had already received unilateral gene therapy (GT) for Leber's Congenital Amaurosis type 2 (LCA2), a rare blinding eye disease. Although an optimal neuroimaging study design would be to capture the baseline brain state of the LCA patients before any intervention (e.g. GT), our neuroimaging protocol, which was conducted independently from the LCA clinical trial, did not occur in parallel. As such, we did not have access to these patients at baseline (before GT). Therefore, the current study is concentrated on comparing the functional and structural differences between visual pathways emanating from the treated and untreated eyes.

Comparing treated and untreated eyes within the same patients, we previously demonstrated the efficacy of GT in LCA2 with measurements of retinal and visual function, as well as functional Magnetic Resonance Imaging (fMRI). Both the retina and visual cortex were much more sensitive to light stimulation in the treated eye as compared to the untreated eye, even after prolonged (up to 44 years) visual deprivation(*1*). Although the enhanced responsiveness of the visual cortex is suggestive of plasticity, it could still simply reflect the engagement of maintained visual pathways following restoration of input. The current study aims to ascertain the role of structural brain plasticity by investigating the impact of visual deprivation and subsequent vision restoration (by GT) on the major visual pathways in LCA2 patients, and how that relates to changes in the functional properties of the cortex.

Numerous animal studies have reported structural changes in visual pathways following the implementation of visual deprivation. For example, dark reared mice or rats have reduced quantities of spines in the pyramidal cells of the primary visual cortex (V1) - potentially due to loss of visual inputs(*8*, *9*). Similarly, unilateral eye closure (UEC) - as first demonstrated by Hubel and Wiesel(*10*) - produces a dramatic reduction in arborization of the geniculostriate (GS) fibers, which serve the deprived eye and terminate in layer 4 of the visual cortex. Subsequent UEC studies further confirmed these initial observations and the remarkable remodeling of the GS fibers due to visual deprivation(*11*, *12*). Recently, Yu and colleagues(*13*) conducted a longitudinal study that tracked visual responses and changes of dendritic spines in the ferret visual cortex following brief periods of UEC. Similar to earlier reports(*13*), improved visual function in the deprived eye was tightly correlated with structural alterations in V1. Parallel to the shrinkage in arborization of neurons in V1 and GS fibers, the majority of UEC studies have also observed an increase in the synaptic terminals serving the open eye(*11*, *13*, *14*). Together, these animal studies demonstrate that visual deprivation leads to a reorganization of the dendritic architecture of V1 cortical neurons. Similar structural changes with visual deprivation have also

been reported in studies of early blind humans, including apparent atrophy of the GS tracts(15) and reduction in the volume(16) and fractional anisotropy(17) of the splenium of the corpus callosum. Thus, it is important to ascertain if the structural changes caused by lack of vision are reversible when vision is restored.

In an attempt to answer this question, many animal experiments first induced UEC and then reversed the process, restoring visual input. Results from these studies have consistently demonstrated that both the structural and functional changes of UEC are largely reversible when the deprived eye is reopened. The most common features of the structural reversibility among these studies have been reported to be within the lateral geniculate nucleus (LGN), V1, or along the GS fibers. For example, Dursteler and colleagues(18) showed a partial regrowth of geniculate cells receiving projections from the deprived eye after only a few days of reverse eyelid suture in kittens. In the monkey, recovery of GS arbors was shown in layer 4 of V1 after reverse suture during the critical period of development after birth(19, 20). In agreement with these aforementioned reports, Movshon and Blakemore(21), in a study of reverse eyelid suture in kittens, demonstrated that GS fibers exhibit a shift in favor of the open, recently unsutured eye 10 days after an initial week of monocular deprivation. Finally, a recent study of UEC and reversal of suture in ferrets(13) reported recovery from UEC to be rapid and robust, occurring within a few hours of eye opening and that as little as 24 hours after eye opening, dendritic spines could return to their pre-UEC numbers(13).

While all the animal studies highlighted so far elucidate specific neuronal underpinnings responsible for changes in visual cortex in response to visual impairment, vision restoration, and environment interactions, similar studies have not been possible in humans due to the invasiveness of the procedures. With access to a group of genotypically and phenotypically characterized subjects with LCA2 who underwent GT and regained visual function, the current study provides a unique opportunity to draw parallels between cortical plasticity changes reported in animal studies with reverse eye-lid suture (regaining sight) and human retinal GT in LCA2 patients (regaining sight).

Distinct from the eyelid suture animal studies where vision is typically restored to the entirety of the retina, the GT in the current LCA2 clinical trial restores vision to specific regions of the retina based on the site of injection of viral vector. As different parts of the retina feed visual input to the brain via distinct visual pathways, this presents an opportunity to separately examine structural and functional changes of these pathways due to continued visual deprivation (untreated retinal areas) and restoration (treated retinal areas). For example, the temporal fibers of the retina signal to the ipsilateral visual cortex, while the nasal fibers cross to the contralateral hemisphere. Thus, subretinal injection to the temporal area of the retina may restore visual input to the ipsilateral V1 through the temporal GS fibers, while injection to the nasal area of the retina may restore visual input to the contralateral V1.

Thus, we hypothesized that restoration of retinal function in LCA2 patients lead to structural changes in both GS fibers and V1 specific to the subretinal injection site. To test this hypothesis, we employed diffusion tensor imaging (DTI) to examine the effect of deprivation and subsequent unilateral retinal GT on the organization and/or reorganization of white matter microstructure in V1, and we used DTI tractography to examine the effect of deprivation and

unilateral GT on the integrity and/or plasticity of white matter fiber bundles connecting V1 to other primary and higher order visual centers in the brain. Finally, cortical activations induced by stimulation of the treated eye in LCA2 patients and the corresponding eye in sighted controls was compared to evaluate functional outcomes resulting from GT.

Our results suggest that visual experience initiated by GT not only enhances functional responses, but may also be responsible for the reorganization and maturation of synaptic connectivity of the visual pathway, leading to mutually dependent structural and functional brain changes.

Results

Our initial analyses focused on cross sectional group differences between LCA2 patients and controls using both voxel-based diffusion parameters and averaged fractional anisotropy (FA) values relative to the principle diffusion direction of the white matter tracts connecting the occipital lobes to other brain areas (tractography). Diffusion results were then correlated with age (reflecting the progression of the disease) and clinical symptoms. All but one of the LCA2 patients received their subretinal injection to the right eye and all 10 subjects received their injection in the superior temporal aspect of their macula/retina. Since projections from the right superior temporal retina remain ipsilateral, not crossing-over in the optic chiasm, the retinal GT should predominantly affect the visual pathways projecting to the right hemisphere. Thus, comparing the diffusion results of the left hemisphere between LCA2 patients and controls can reveal the effect of continued deprivation on the structural properties of the visual pathways, while the results from comparing the left and right visual pathways within LCA2 patients provides a measure of the impact of retinal GT.

Asymmetric Compromised White Matter Microstructure (L>R) in the Primary Visual Areas in LCA2 Patients

Results of Voxel-Based Analysis (VBA) for FA of the LCA2 patients compared with the sighted control group revealed a number of clusters of reduced FA within both the right and left occipital lobes (Fig.1A, column 1, yellow clusters). Reduced FA clusters were superimposed onto the color FA population-based atlas constructed from all study participants (N=21). As shown in the axial views of Fig. 1, section A, reduced FA clusters were located bilaterally in the occipital cortex with larger clusters in the left (3272 significant voxels) than right (2301 voxels) hemisphere. A Chi square test of these counts revealed a highly significant difference (Chi-square = 169.2, $p < 0.001$) from a symmetrical distribution. Reduced FA clusters were mainly situated in the vicinity of the calcarine fissure (Brodmann Area 17 & 18) and are clearly shown on sagittal images of Fig. 1 (white arrows), section A. An additional reduced FA cluster for LCA2 patients was found in the splenium of the corpus callosum (Fig. 1B), a location known to be involved in binocular vision, through which fiber bundles (occipital-callosal fibers) connecting the left and right occipital cortices pass (*3*). VBA did not reveal any clusters with increased FA at the same statistical threshold.

Water diffusivity relative to the principle diffusion direction of the fibers is called axial diffusivity (AD), the component of diffusivity relative to the direction perpendicular to the principal direction is called radial diffusivity (RD), and the measure of the average diffusivity in all directions is called mean diffusivity (MD). LCA2 patients showed clusters of increased RD (Fig.

1A, column 2, blue clusters). Similar to the FA results, increased RD clusters were also primarily located in the medial aspect of the visual cortex and distributed in and around the calcarine fissures (near V1). LCA2 patients also showed increased MD (Fig. 1A, column 3, blue clusters), again bilaterally distributed and medially located in visual cortex near the calcarine fissure. Finally, analysis of AD did not reveal significant clusters of abnormality for the LCA2 patients as compared to the control group. Collectively, VBA results of the primary diffusion indices of FA, RD, and MD for LCA2 patients as compared to sighted controls suggest compromised white matter microstructures for LCA2 patients in bilateral primary visual cortices (V1 areas) with stronger effects in the left than right hemisphere (see Fig. 1, section A) and the splenium of the corpus callosum. Detailed information on the centroid coordinates of clusters' size and locations along with their Brodmann areas (BA) in the Montreal Neurological Institute (MNI) template (http://neuro.debian.net/pkgs/fsl-atlases.html) for all diffusion parameters (FA, RD, and MD), obtained from the voxel-based analysis of LCA2 group compared with the sighted controls, are presented in Table 1. The mean and standard deviations of the average diffusion parameters for clusters in the left and right visual cortices are shown in Table 2.

Previous reports from animal and human studies(*22*, *23*) have shown that a combination of decreased FA and increased RD and MD (Table 2) without significant changes in AD may be indicative of demyelination, or reduced/arrested myelination.

Importantly, VBA additionally revealed that the compromised white matter microstructures showed a distinct asymmetric pattern. In particular, as shown in Table 2, LCA2 patients presented with lower FA and higher RD and MD values for the left as compared to their right visual cortex, whereas diffusion parameters for sighted controls were roughly similar for both occipital cortices. It is important to note that we included all patients (9/10 treated in the right eye and 1/10 treated in the left eye) in the group analysis, comparing LCA2 patients with demographically matched controls. While the group VBA results showed more compromised white matter in the left, for the one subject who received subretinal injection in the left eye, diffusion results were clearly reversed. As shown in Table 2, average FA for the right occipital FA was 0.260 and 0.252 for controls and LCA2 patients respectively with no significant differences. On the other hand, the right occipital FA value for the one subject treated in the left eye was 0.18, which is different from the FA values reported for both the LCA2 and control groups. Similarly, the values for the left occipital FA were 0.252 and 0.199 for controls and LCA2 patients as whole respectively, whereas FA value for the left occipital cortex for the one subject treated in the left eye was 0.23, demonstrating a clearly reverse pattern of asymmetry from the group.

In an additional analysis, the average FA values from two regions-of-interest (ROIs) in the primary visual cortex (calcarine area) of both hemispheres were compared between the LCA2 and controls revealing significant differences between the left and right ROIs in the LCA2 patients, but not controls, and a significant difference between the two groups for the left ROI only. The ROI analyses showed left average FA values of 0.129 and 0.161 for the LCA2 and controls respectively ($p < .017$). Results for the average FA of the right ROI was 0.142 and 0.168 for LCA2 patients and controls respectively ($p > 0.23$). Of note is that the left and right mean FA for the calcarine ROIs of the one subject injected in the left eye was 0.166 (left) and 0.142 (right), respectively. Similar to the VBA results, the ROI results also show an increased FA within the visual cortex ipsilateral to the treated eye.

These observed asymmetries may be due to the fact that unilateral ocular GT (in the

temporal retina of the right eye in nine subjects and temporal retina of left eye in one subject) predominantly affected the visual pathways projecting to the ipsilateral hemisphere of the treated eye and not the fibers decussating to the contralateral side. This asymmetry in VBA findings of LCA2 patients was later closely examined in the whole group by further performing tractography and analyzing the white matter integrity along the left and right geniculostriate tracts.

Our results are consistent with reports on humans with early or congenital blindness(*15-17*, *24-26*) that found significant disruptive WM changes especially in the primary visual cortex when compared with matched sighted controls.

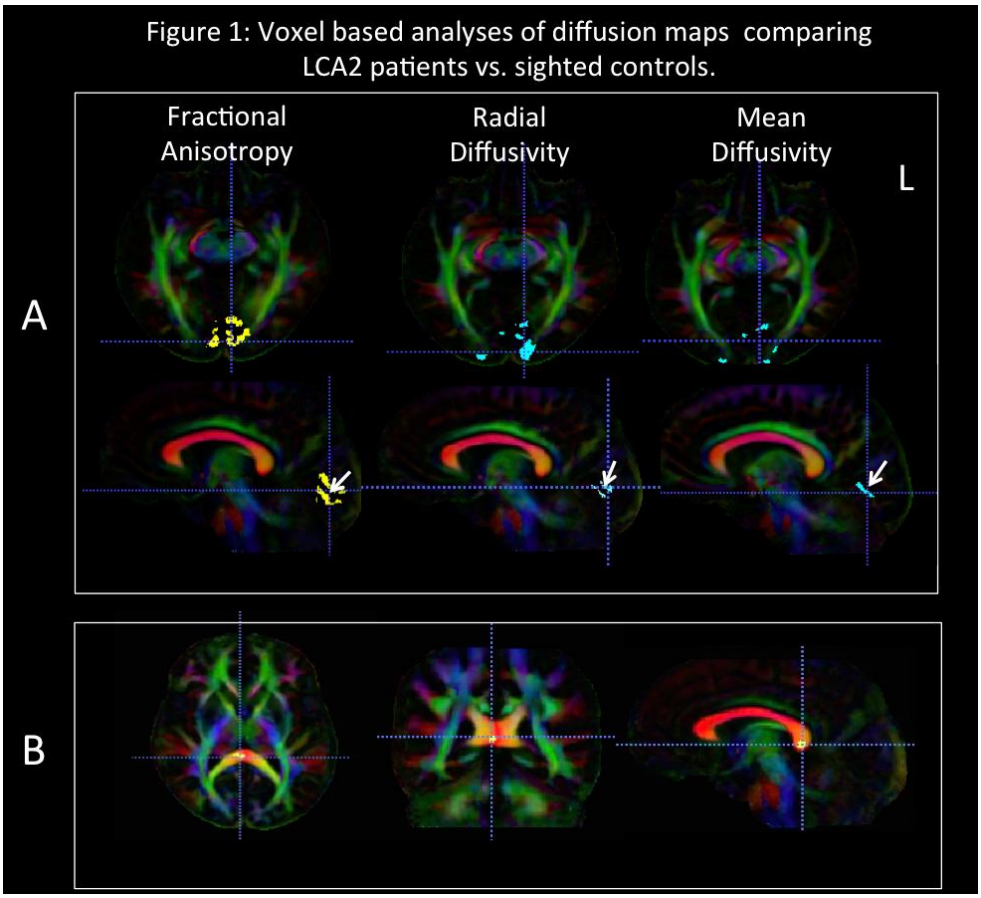

Fig. 1: Voxel based analyses of diffusion maps comparing LCA2 patients vs. sighted controls. Section A; Voxel-based analysis (VBA) results of LCA patients vs. demographically matched normal sighted controls are shown for three diffusion parameters of fractional anisotropy (FA), radial diffusivity (RD) and mean diffusivity (MD). VBA results are superimposed onto the color FA population based atlas constructed from all study participants (N=21). In the first column, the VBA results for FA reveal yellow areas (arrow) that show decreased FA for greater than 100 contiguous voxels that are significant after corrections for multiple comparisons (false discovery rate (fdr) $q<0.05$). Axial images (top row) show larger clusters with reduced FA in the left V1 (4211 Voxels) as compared to the right (1853 Voxels). Sagittal images (bottom row) are presented to demonstrate that the reduced FA clusters within the visual cortex are primarily located in and around the calcarine fissure (arrowhead), which also is known as the primary visual area (Brodmann Area 17 & 18). In the second column, VBA results for increased RD are shown, at the same statistical threshold for FA, in

Cluster Locations	MNI Coordinates (Centroid)			Cluster Size (# of Voxels)
FA	X	Y	Z	
Lt. Visual cortex (BA-18)	-6	-103	-5	1824
Rt. Visual Cortex (BA-17)	19	-80	5	1580
Lt. Visual Cortex (BA-17)	-3	-88	1	1448
Rt. Visual cortex (BA-18)	24	-102	-2	378
Rt. Visual cortex (BA-19)	43	-80	-2	343
Splenium of Corpus Callosum	7	-34	12	100
RD				
Lt. Visual cortex (BA-17)	-12	-81	13	1495
Rt. Visual Cortex (BA-18)	7	-81	-1	813
Rt. Visual Cortex BA-17	10	-79	7	136
Lt. Visual cortex (BA-17)	-2	-82	7	100
MD				
Rt. Visual cortex (BA-19)	20	102	-3	601
Lt. Visual Cortex (BA-17)	-6	-94	3	540
Rt. Visual Cortex BA-17	11	-72	6	138
Lt. Visual cortex (BA-17)	-2	-80	12	120
Lt. Visual cortex (BA-19)	-32	-86	17	118

Table 1. Size and center of mass (Centroid) MNI coordinates of the FA, MD and RD significant clusters extracted from voxel based analyses of diffusion maps

Clusters Location	LCA2 Patients	Normal Sighted Controls
	Mean FA (SD)	**Mean FA (SD)**
Rt. Occipital	.202 (.018)	.260 (.022)
Lt. Occipital	.199 (.024)	.252(.025)
Splenium	.660 (.034)	.711(.028)
	Mean RD (SD) (10^{-6} s/mm^2)	**Mean RD (SD) (10^{-6} s/mm^2)**
Rt. Occipital	743.0 (38.6)	679.5 (27.2)
Lt. Occipital	822.0 (48.8)	730.9(43.1)
	Mean MD (SD) (10^{-6} s/mm^2)	**Mean MD (SD) (10^{-6} s/mm^2)**
Rt. Occipital	816.0 (39.5)	757.3 (36.4)
Lt. Occipital	860.0 (47.8)	783.0 (42.3)

Table 2: Averaged diffusion indices (mean and standard deviation) for the significant clusters (reported in Table 2) resulted from group voxels based analyses of diffusion maps of LCA2 patients and sighted controls.

The above VBA and ROI analyses clearly demonstrate a reverse normalization process for the occipital microstructural white matter for patients treated in the right versus the one subject treated in the left eye. In the remainder of this article, further tractography and correlational analyses will be focused only on the 9/10 subjects treated in the right eye to insure sound and unbiased statistical results.

White Matter Microstructure in Primary Visual Areas of LCA2 Patients Does Not Follow the Same Life-Span Trajectory as Sighted Controls

LCA is known to occur bilaterally, affecting both eyes symmetrically(*27*, *28*) and thus, the disease should affect both visual cortices. LCA is a degenerative disease(*28*, *29*) and, although there is variability contributed by the fact that each individual in our study (except for a pair of twins) has different *RPE65* mutations and each has different environmental exposures, age can be considered a proxy for disease progression. A case report showing a clear correlation between degree of retinal/visual function in an LCA2 patient and age supports this premise(*30*). As such, separate Spearman correlations were performed between the age and the average FA (from the significant clusters with reduced FA) of the left and right occipital cortices (Fig. 2). No correlations between FA and age were observed for the left ($R=0.10$; $p<0.770$) or right ($R=0.155$; $p<0.650$) occipital clusters for the control subjects. This maturational trajectory of the occipital FA with age for control subjects, as shown in Fig. 2, is consistent and inline with previous reports. For example, examining age-related changes for FA in various brain regions, Salat et al(*31*) and

Davatzikos et al(32) reported that occipital fibers are myelinated at an early age and are relatively preserved over time. While LCA2 patients demonstrated a similar absence of correlation with age for their right occipital FA (R= - 0.467; p< 0.25), their left occipital FA showed negative correlation with age (R= - 0.633; p<0.067), as depicted in the top two panels on the left side of Fig. 2. A direct comparison of groups showed a trend for differences in correlation between the two groups for the left but not right occipital FA (Fisher test, $p < 0.058$ and $p > 0.10$, respectively). The asymmetry in the correlations of FA with age (albeit at trend level) is consistent with the asymmetry observed in the VBA results (see Fig. 1A). The decline of the occipital FA with age may be attributed to the degenerative nature of the LCA2 disease, which in turn would lead to further disuse of the visual cortex over time.

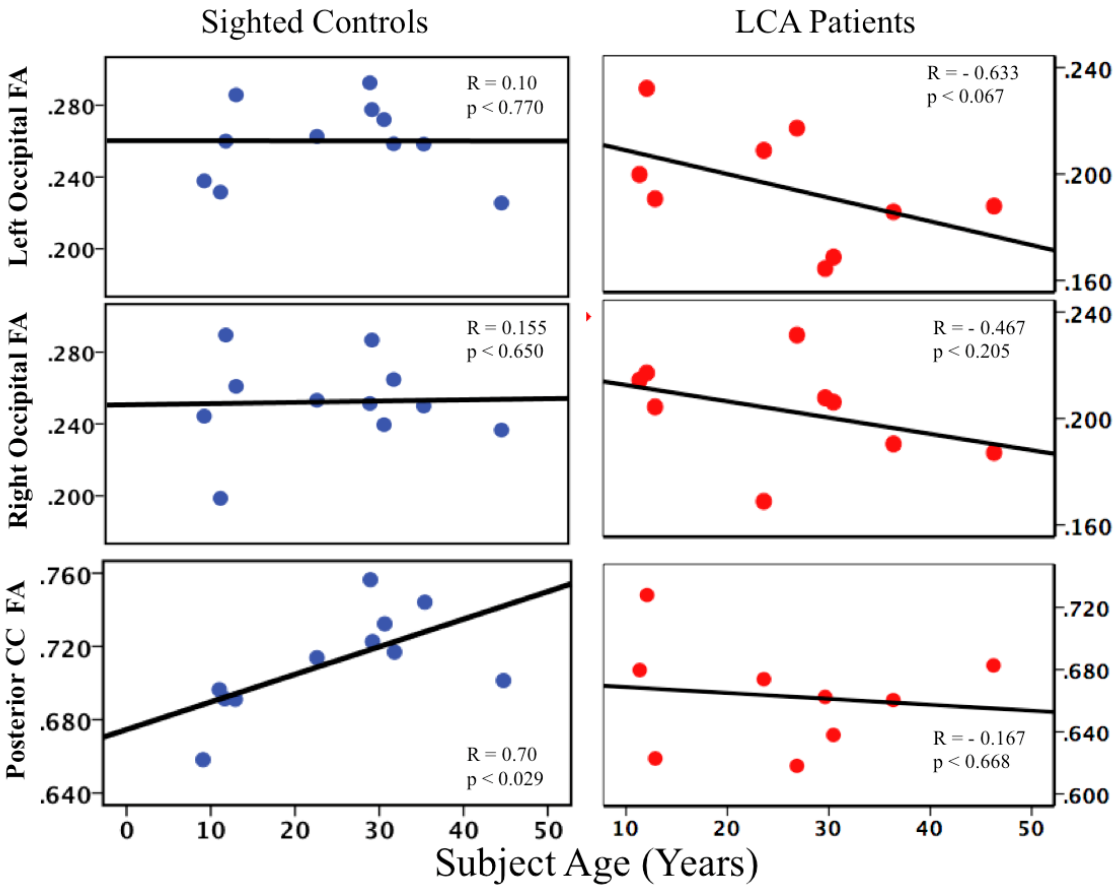

Fig. 2: Spearman correlations of occipital FA with age. Spearman correlations of subjects' age with the average FA for the right and left clusters of abnormalities in the occipital cortex and posterior corpus callosum are shown. While LCA2 patients demonstrated similar correlations to those of normals for the right occipital FA, their left occipital FA was negatively correlated with age demonstrating a continuous decline of the left primary visual area for these patients. However, posterior CC FA correlation with age was noticeably different for the LCA2 patients. Absence of positive correlation for the FA and age in the splenium of the CC for LCA2 patients maybe due to the progressive nature of the disease signifying the decline in communication between the two visual cortices over time and reduction in the number of fibers crossing the splenium connecting the left and right occipital cortex.

The lower panel in Fig. 2 shows the age-related changes of FA for the posterior corpus callosum (CC) for both LCA2 (left panel) and sighted controls (right panel). Control subjects presented strong and significant positive correlations between posterior CC and age (R=0.70; p<0.029), which is consistent with reports on the FA of CC and its positive correlation with age for normal aging subjects(*33*). However, the LCA2 subjects showed no correlations with age for this region (R= - 0.167; p<0.67) and once again showed deviation in their microstructural white matter development over their life-span trajectory. Direct comparison between groups showed that the difference in correlation for the posterior CC FA was significant (p < 0.028).

In summary, age correlations with FA in sighted controls are consistent with previous reports on the occipital cortex(*31*, *32*) and CC(*33*). The correlation results for LCA2 patients are suggestive of greater effects of GT on the right visual cortex (V1) as compared to the left, a trend that is consistent with the results of VBA (Fig. 1A).

Relationship Between Gene Therapy Treatment Time and Integrity of White Matter Microstructure in the Visual Cortex

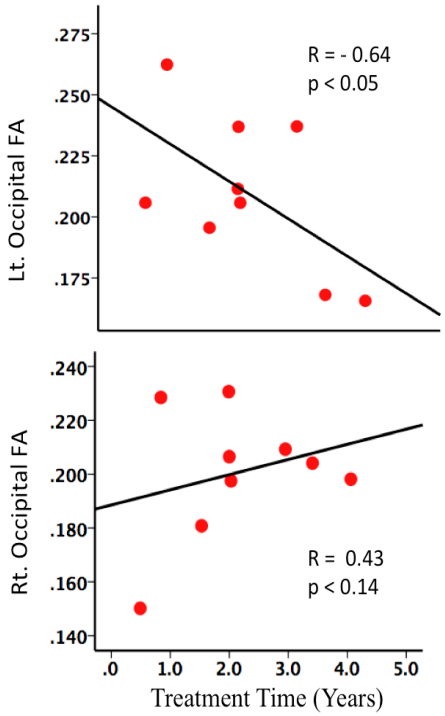

Fig. 3: Spearman correlations of the left and right occipital FA with patients' treatment time. Left and right occipital FA was correlated with number of years of treatment (years after GT) for subject treated in the right eye at the time of his or her MRI scan. Results showed significant negative correlations (R = - 0.64, p < 0.05) for the left occipital FA and a trend toward a positive correlation (R = 0.43, p < 0.14), albeit not significant, for the right occipital FA and treatment time. Furthermore, there was a significant difference between the left and right occipital FA with respect to their correlation with treatment time (p < 0.003, Steiger's test for dependent correlations)(*2*).

To further examine the effect of retinal GT on white matter microstructure of the visual cortex, we performed correlational analysis between the average FA values of the right and left VBA reported clusters of diffusion abnormalities (Tables 1&2) as a function of the amount of time between the administration of GT and the MRI scans (9/10 patients). As shown in Fig. 3, the left FA values depict significant negative correlations with time post GT whereas the FA values for the right visual cortex are not negatively correlated. In fact, they show a trend toward improvement (slight positive slope) with time post intervention. Furthermore, there was a significant difference between the left and right occipital FA with respect to their correlation with

treatment time ($p < 0.003$, Steiger's test for dependent correlations)(2). These results show strong asymmetry in the values of the right and left white matter microstructures of the visual cortex, a finding consistent with above reported correlations of FA and age.

Patients' Amplitude and Frequency of Nystagmus Correlate with Compromised White Matter Microstructure in Left V1

Exploratory Spearman partial correlations (covaried for age) were performed to evaluate possible relationships between the reduced FA clusters within the left and right occipital cortices and several clinical measures including visual acuity, visual field, full field sensitivity, and amplitude and frequency of nystagmus (9/10 patients). The only clinical symptoms that significantly correlated with FA values (Bonferroni corrected $q = 0.05/14 = 0.0036$) were the frequency and amplitude of nystagmus for both eyes (Fig. 4). In particular, the left occipital FA values showed significant correlations with amplitude of nystagmus in the right ($R = -0.98$, $p=0.002$) and left ($R = -0.92$, $p=0.01$) eyes as well as the frequency of nystagmus in both the right ($R = -0.96$, $p=0.002$) and left eyes ($R = -0.95$, $p=0.004$).

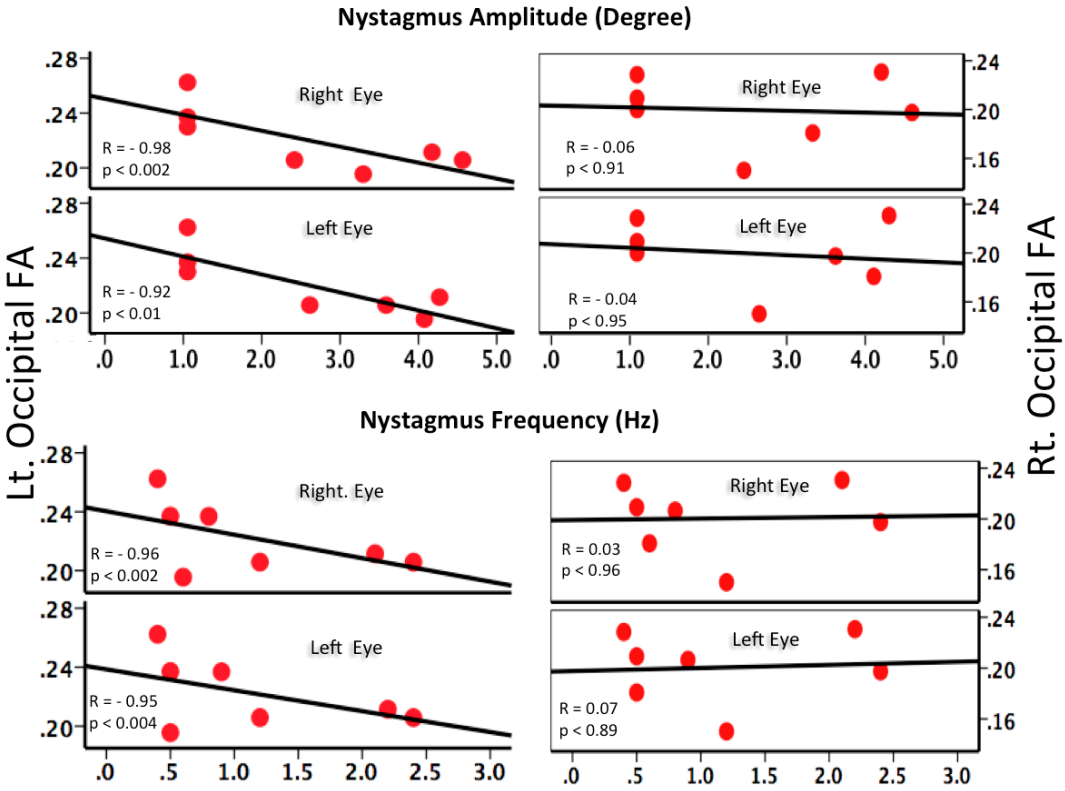

Fig. 4: Spearman correlations of occipital FA with patients' amplitude and frequency of nystagmus. Correlation results for the left and right occipital FA and the nystagmus frequency and amplitude of the left and right eyes of LCA2 patients. As shown here, nystagmus characteristics for either the right or the left eye are not correlated with the integrity of visual fiber bundles within the right occipital cortex. On the other hand, there exist strong and significant correlations between the FA of the left visual cortex and nystagmus characteristics of both the left and right eyes. Data is shown for patients treated in the right eye (9/10) with nystagmus information mission for two subjects.

Visual Pathways Show Asymmetric Disrupted Connectivity in LCA2 Patients as Demonstrated by Fiber Tractography

Collectively, results from animal studies(*13*, *18-20*) and early blind human studies(*15*), report effects of visual deprivation and its reversal on LGN, V1 and the GS fibers. To examine the effects of long-term deprivation and restoration of vision on the GS tracts (connecting LGN to V1) as well as other fibers connecting the occipital cortex to the rest of the brain in LCA2 patients, we conducted diffusion fiber tractography. The average FA along the left and right white matter fiber bundles terminating in the occipital cortex (including inferior longitudinal fasciculus (ILF), occipitocallosal (OC), and inferior fronto-occipito fasciculus (IFO), as well as

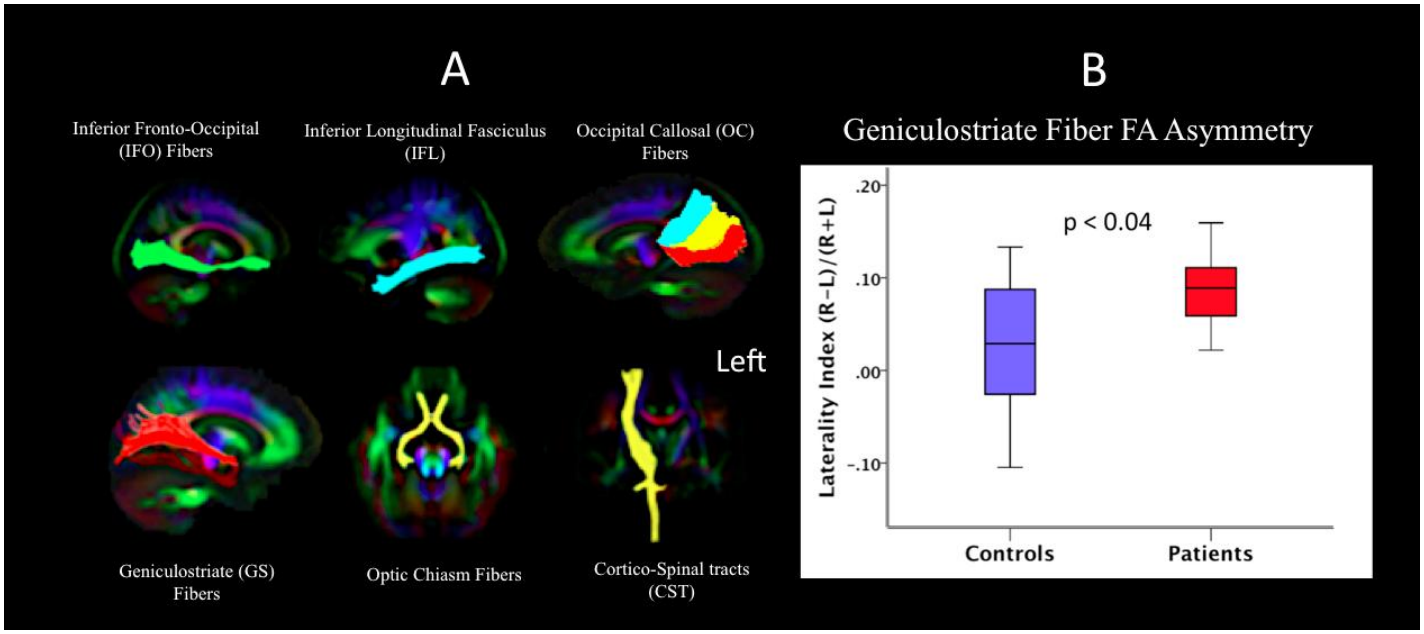

Fig. 5: Fiber tractography results. Panel A: Using DTIStudio tractography software and population specific template, major fiber tracts connecting the occipital cortex to the rest of the brain such as the inferior fronto-occipital (IFO), inferior longitudinal fasciculus (ILF), occipito-callosal (OC) and, geniculostriate (GS) as well as chiasm tracts were extracted bilaterally. Following Dougherty et al (*3*) the OC fibers were extracted by placing three ROIs in the upper, middle, and lower areas of the inferior portion of the splenium to extract tracts that end in dorsal V3 visual areas (blue), dorsal and ventral V1 and V2 (yellow), and ventral V3 and V4 (red). In addition to vision related tracts, bilateral corticospinal tracts (CST) were extracted as control fibers. Tractography analyses of all these tracts showed no difference between the LCA2 patients and sighted controls except for the GS fibers. The averaged FA along the right GS fibers for the LCA2 patients did not differ from the control group ($p=0.389$); however, tractography results showed significantly decreased FA along the left GS fibers ($p = 0.0045$). Panel B: Laterality index (R-L) of the average FA along the left and right GS fibers for the LCA2 patients and controls were evaluated according to laterality index ((Rt. GS avg. FA - Lt. GS avg. FA) / (Rt. GS avg. FA + Lt. GS avg. FA)). LCA2 patients showed much higher average FA value for the right GC fibers and their laterality index (red bar) significantly ($p<0.04$) differed from their matched controls (blue bar).

optic chiasm fibers) was assessed. Assessment was also carried out for the corticospinal tracts (CST) that do not terminate in the occipital cortex. These were viewed as control fibers. Extracted tracts for IFO, ILF, OC, GS, optic chiasm, and CST fibers are presented in Fig. 5A. Tractography analyses of all these tracts showed no difference between the LCA2 patients and sighted controls,

except for the GS fibers (Table 3, Bonferroni corrected alpha = 0.05/12 = 0.0042). To investigate the effects on the GS fibers more closely, we conducted an ANOVA using hemisphere as a repeated measures factor, group as a between-subjects factor and age as a covariate. This analysis revealed a significant main effect of group ($p < 0.042$) as well as a significant interaction between

group by hemisphere ($p<0.044$). Further, post-hoc t-tests revealed significant difference

between groups for the left ($p < 0.0045$) but not right GS fibers ($p > 0.389$). These results confirm a specific difference between patients and controls for the untreated side (see Table 3). We further computed a laterality index ((Rt. GS avg. FA - Lt. GS avg. FA)/ (Rt. GS avg. FA + Lt. GS avg. FA)) of the averaged FA along the right and left GS fibers between the LCA2 patients and demographically matched controls (Fig. 5B) demonstrating a significantly ($p<0.04$) larger laterality index in the LCA2 patients as compared to their matched controls. Tractography results also suggest that cortico-cortical connections between the visual cortex and the rest of the brain are well preserved in the LCA2 subjects, as no differences were observed as compared to the demographically matched controls.

Avg. FA	Groups	Mean	SD	***p***
Right GS	Sighted Controls	.417	.036	.389
	LCA2 Patients	.413	.019	
Left GS	Sighted Controls	.397	.041	.0045
	LCA2 Patients	.346	.045	

Table 3: Statistical comparison of the average FA measurement for the right and left geniculostriate fibers of LCA2 patients treated in the right eye (controlled for age) as compared to sighted controls.

In summary, tractography results were consistent with VBA results and Spearman correlations of FA with age. Based on VBA, tractography, and age correlation, results suggest a normalization process within V1 and GS fibers of the right hemisphere initiated by GT in the superior temporal macula/retina. To further test this hypothesis we next examined the existence and degree of functional asymmetry of the visual cortex in response to GT as compared to the distribution of cortical activations observed in sighted controls.

LCA2 Patients Show Similar Asymmetry in Their Visual Cortical Activation Patterns as the Asymmetry Observed in Their Geniculostriate Connectivity

The structural MRI data presented above suggest that GT applied to the temporal retina of the right eye reverses structural changes in the right GS fibers that were caused by visual deprivation. In order to examine whether functional brain responses follow the structural changes brought about by GT and show a similar normalization along the right GS tract, a retrospective analysis was performed to compare fMRI results of LCA2 subjects to the average response from

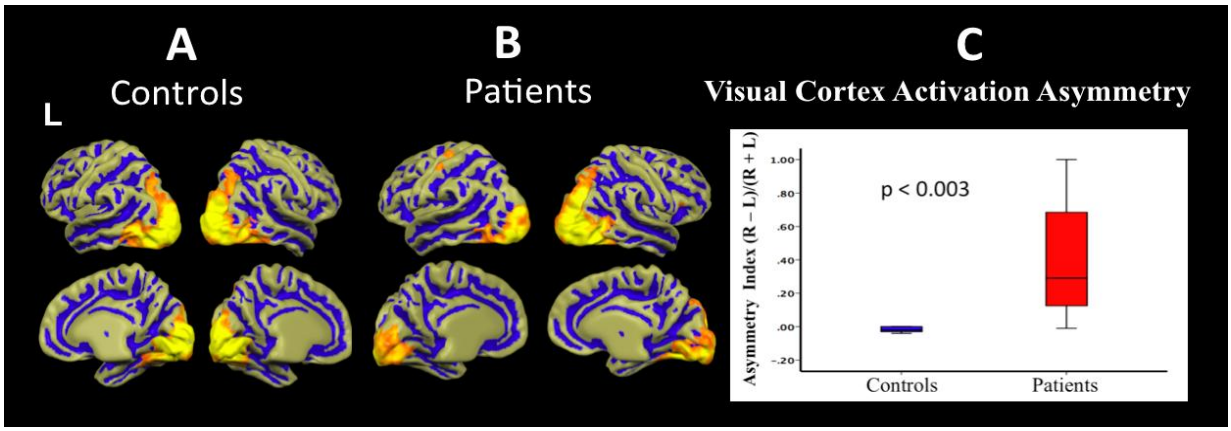

Fig. 6: Group Averaged fMRI Results: Group averaged fMRI response of the right eye in response to the high contrast checkerboard stimuli(*1*) in sighted controls and LCA2 patients. A symmetrical distribution of activation in both hemispheres for sighted controls as opposed to a clearly asymmetric distribution for LCA2 patients is shown. As shown in Panel C, the cortical activation laterality index defined as (Rt. Total visual cortex activation volume – Lt. visual cortex activation volume) / (Rt. Total visual cortex activation volume + Lt. Total visual cortex activation volume) is significantly larger ($p<0.003$) for LCA2 patients as compared to sighted controls.

the control group. Fig. 6A shows the group-averaged fMRI results for right eye stimulation of 9 matched sighted controls demonstrating a near symmetrical hemispheric activation distribution in response to the checkerboard paradigm(*1*, *34*). This is expected from the connectivity of the human retina to the brain(*35*) with each eye connected roughly equally to both hemispheres (53% of axons decussate in the optic chiasm). In contrast, group averaged fMRI results for the right eyes of the 9 LCA2 patients, as shown in Fig. 6B, depict significantly larger cortical activations in the right hemisphere as compared to the left in response to the same visual stimuli. This asymmetry of cortical activation in LCA2 patients (R>L) follows a similar pattern of the asymmetry we observed for the averaged FA values along the GS fibers (R>L). To further quantify this asymmetry, volume of

Cortical Activations	Groups	Mean $(mm)^3$	SD $(mm)^3$	*p*
Right Occipital	Sighted Controls	29415	14682	.32
	LCA2 Patients	22129	13254	
Left Occipital	Sighted Controls	30141	14672	.05
	LCA2 Patients	15143	13348	

Table 4: Statistical comparison of the total volume of activations within the right and left visual cortices between LCA2 and sighted normal groups.

cortical activations distributed over the entire right and left visual cortices were calculated for both the LCA2 and control subjects (Table 4). A laterality index was then obtained: ((Rt. Total # of Activation Voxels – Lt. Total # of Activation Voxels)/ (Rt. Total # of Activation Voxels + Lt. Total # of Activation Voxels). As depicted in Fig. 6C, the laterally index for the total visual cortex activations induced from stimulation of the right eye in LCA2 and matched sighted controls subjects using the same high contrast checkerboard stimuli, is significantly greater for the LCA2 patients ($p<0.003$).

Discussion

Human LCA2 patients treated with subretinal gene therapy have experienced significant and continual visual improvement over time. These improvements have been mostly attributed to the rescued retinal cells, but vision develops from the joint collaboration between the eye and the brain. Focusing on a group of visually impaired LCA2 patients who had received unilateral temporal retinal GT (in their worse seeing eye), we report strong evidence for structural plasticity in the visual pathways ipsilateral to the treated retina. First, consistent with prior reports in animal(*8*, *9*, *11*, *14*, *18*, *19*, *36*) and blind human studies(*15*, *25*, *37*) we found impaired structural properties of the visual pathways compared with matched controls, suggesting atrophy of the visual pathways following extended visual deprivation. Critically, however, these structural differences were asymmetric, with reduced differences between the LCA2 patients (9/10 treated in the right eye) and controls in the right occipital cortex compared with the left, corresponding closely with the projections from the site of sub-retinal gene vector administration. Furthermore, for the one subject who received treatment to the left eye this effect was reversed with the left occipital cortex showing normalization. This group structural asymmetry was observed in voxel-based, tractography, and correlational analyses and was further supported by an asymmetry in the functional responses of the visual cortex. Collectively, our findings suggest that restoration of retinal function may lead to strengthening of the visual projections into the cortex. The type of structural changes seen in our current study are similar to those reported in a recent report on the relationship between the integrity of white matter tracts of the visual system and cortical function in a group of patients with compression of the optic chiasm by pituitary gland tumors and recovery of visual abilities after surgical removal of the tumor and subsequent decompression of the visual fibers(*38*). Authors showed that compression of the optic chiasm led to demyelination of the optic tracts and the severity of demyelination in patients predicted visual ability and functional activity of the primary visual areas. Furthermore, subsequent to decompression of optic chiasm, rapid regeneration of myelin in the human brain was observed which was closely correlated with cortical visual activities, and ultimately the recovery of patients' visual function(*38*). Results from this study are highly relevant to the current report as the authors clearly demonstrate human brain plasticity depicted in remyelination process of the visual fibers and a direct relationship between the degree of remyelination and patients' visual ability.

Although the optimal neuroimaging study design for the evaluation of the effects of GT on human brain would be to capture the baseline brain state before any intervention (e.g. GT), our neuroimaging protocol was conducted independent from the LCA clinical trial and started after the LCA trial had initiated. Thus, we did not have access to these patients at baseline (before GT). While this is a limitation of the current study, by comparing functional and structural differences between the treated and untreated eyes, the data reveal important insights into brain plasticity after restoration of vision.

Similar to the results reported by the Paul and colleagues(*38*), the structural and functional changes we observed could be due to increased myelination of V1 and GS fibers, which in the case of GT are thought to depend on life experiences and environmental interactions(*39*). For example, Ishibashi et al(*40*) reports that repeated electrical stimulation of axons results in an increase in myelination. And more recently, considerable structural plasticity was reported in the brains of gorillas living in a naturalistic environment as compared to ones who were caged. Also, living in different habitats with semi-naturalistic environments alters brain structure in adult marmosets(*41*). Not only did animals living in more complex environments have more connections between neurons, but they also exhibited a higher rate of neurogenesis than their caged control counterparts. Consistent with these reports, our results demonstrate that reversing blindness through GT, and the subsequent increase in visual experiences and interaction with environment, promote long-term structural plasticity, which in turn further enhance visual function (see structural and functional asymmetry index, Figs. 4C&5C respectively). Although vision results from a collaborative effort between the eye and the brain, the degree of the brain's involvement in securing long-term preservation and improvement of what was initiated by retinal gene delivery has not yet been carefully examined and deserves closer investigation. Evidence for changes in white matter structure through training has been reported in other cross-sectional and longitudinal studies in humans. For example, Bengtsson and colleagues(*42*) reported differences in the spinothalamic tract between musicians and non-musicians. Similarly, changes in white matter structure have been reported in subjects training to juggle(*43*) or performing a balancing task(*44*) over several weeks. Thus, it is plausible that LCA2 patients involved in future retinal GT studies may benefit from exercises designed to enhance the use and function of the visual pathway.

Study Limitations

The major limitation for the current study is lack of access to the baseline brain state of LCA2 patitents before any intervention (e.g. GT). This limitation was due to the fact that the neuroimaging study component was conducted independent from the LCA clinical trial and started after the LCA trial had initiated. Despite this limitation, however, by comparing functional and structural differences between the treated and untreated visual pathways, the data reveal important insights into brain plasticity after restoration of vision. Another constraint is the limited correlations observed for the white matter integrity value of FA and patients' clinical symptoms. Although white matter microstructural abnormalities showed correlations with nystagmus, no correlations were detected for main visual parameters such as visual acuity and visual fields. Inclusion of participants with ages ranging from 11- 47 years may be an additional limitation when studying white matter due to significant maturation process across such wide age span. However, as reflected from results presented here (see Fig. ??) and reported by Salat et al(*31*) and Davatzikos et al(*32*) occipital fibers are myelinated at an early age and are relatively preserved over time.

Conclusions

In conclusion, results from diffusion tensor imaging, diffusion tractography, and fMRI along with the strong correlations of those results with patients' nystagmus measures, age, and length of time post treatment suggest that retinal GT may indeed promote re-myelination of axons of geniculostriate fibers as well as local changes within the primary visual cortex favoring

the treated eye. These observations also suggest that the functional plasticity that we previously reported for LCA2 patients receiving retinal GT (*1*, *34*) may be related to structural changes in the brain. Thus, retinal GT and structural remodeling of the primary visual cortex and GS fibers may indeed be joint processes necessary to sustain long term restoration of visual function. However, longitudinal neuroimaging studies capturing the baseline brain state (pre-GT) are also essential to broaden our knowledge of the effects that retinal gene and/or cell therapy may have on the human visual cortex or the central nervous system as a whole. Such a longitudinal design will also shed light on timing of the plasticity process.

Methods

Leber's Congenital Amaurosis (LCA)

LCA is a rare retinal degenerative blinding disease, usually inherited in an autosomally recessive fashion, with no available cure. It is symptomatic at birth or in the first few months of life, and affects around 1 in 81,000 people(*45*) LCA has been associated with mutations in at least 18 different genes. Mutations in the gene encoding retinal pigment epithelium-specific protein 65kDa (RPE65) are involved in one of the more common forms of LCA - LCA type 2 (LCA2). LCA2 patients are good candidates for gene transfer therapy as the degeneration of their retinal cells is slow, increasing the probability of successful gene transfer to the remaining (although sickly) retinal cells. There are several active clinical trials evaluating gene augmentation therapy for LCA2 patients (www.clinicaltrials.gov) and our subjects had been enrolled in study NCT00516477.

Study Participants

Participants in the clinical trial consisted of 12 LCA2 patients, many of whom had more advanced retinal diseases than the child participants (4/12) (*46*, *47*). One of the FDA mandates for the phase I clinical trial was for GT to be administered in the patients' worse seeing eye. As such, comprehensive psychophysical examinations were performed to identify and document the worse seeing eye in all clinical trial patients. The initial enrollment of older subjects was mandated by the FDA to protect children from the unforeseen complications of the first retinal GT clinical trial in human. The initial subjects enrolled were 3 adults(*46*). Following the demonstration of safety and efficacy of GT in this group, additional subjects, including four children, received the intervention. However, still the worse seeing eye was treated in light of potential risk/benefit ratios. In the current manuscript, we present the neuroimaging evaluation from 10/12 LCA2 patients enrolled in the Phase-I clinical trial. Comprehensive clinical evaluation of all patients determined the worse seeing eye to be the right eye for 9/10 patients and the left eye for 1/10 patients. The patients (6 male) received subretinal injection of AAV2.hRPE65v2(*46*, *47*) in the worse eye ≥ 2 years prior to their MRI study. Eleven sighted control subjects who were demographically

Demographics	Sighted Controls	LCA2 Patients	Statistics
N	11	10	
Males	8	6	Fisher's exact = .93
Avg. age (yrs)	24.37 (11.77)	23.89 (12.32)	t-test > 0.83
Age range (yrs)	9.50-46.24	9.08-44.75	
Right-handed	11	9	Fisher's exact = 0.48
Avg. time bet. GT & Imaging	N/A	2.09 (1.11)	

Table 5. Subject demographics.

matched (8 males) were recruited by flyers and word of mouth. Controls were excluded if they had any current or past psychiatric diagnosis or a history of drug or alcohol abuse. Additional exclusion criteria for all subjects included mental retardation, known neurological disorder, a history of head injury or any focal findings revealed by MRI, or current use of psychotropic medications. Table 5 summarizes the overall characteristics for matching of LCA2 patients and controls.

Gene Therapy Parameters

Subjects	Age at MRI (yrs)	MRI: Time Post Intervention (yrs)	Sex	Treated Eye	Visual Acuity (LogMAR)		Visual Fields at MRI (Sum total degrees at each meridian)		*RPE65* Mutation
					Right	Left	Right	Left	
CH06	23.59	2.95	F	Right	1.74	1.36	337	303	IVS1+5g>a/L341S
CH08	12.75	1.99	M	Right	1.44	0.72	741	454	F530fs/F530fs
CH09	11.34	1.45	M	Left	0.76	1.03	303	929	R124X/Lys297del1aggA
CH10	14.06	2.03	M	Right	1.25	1.07	1257	1283	IVS1+5g>a/Phe530del1ttc
CH11	27.98	2.00	F	Right	0.76	0.65	1304	1012	V473D/V473D
CH12	47.40	1.53	F	Right	2.5	3.0	51	44	K303X/W431C
CH13	37.92	0.49	M	Right	1.61	1.53	523	112	IVS1+5g>a/IVS1+5g>a
NP01	29.63	3.4	F	Right	1.60	1.77	122	76	E102K/ E102K
NP02	30.45	4.1	M	Right	1.64	1.0	45	43	E102K/ E102K
NP15	13.30	0.84	M	Right	0.6	0.47	1371	1208	D167W/H313R

Table 6. Detailed summary of LCA2 patients' demographic along with their visual acuity and visual fields clinical results at the time of MRI scan.

A summary of information regarding the LCA2 patients, gene mutation, age, gender, side of injections, as well as their clinical visual testing for visual acuity and visual fields are presented in Table 6. Detailed information of clinical presentations of these patients who were evaluated as part of Phase I LCA2 clinical trial are presented elsewhere(*47*). In summary, all 12 patients who received unilateral GT showed considerable improvement in their retinal function. The majority of patients showed sustained improvement in several assessments of their retinal/visual functions such as light sensitivity, pupillometry, visual acuity, nystagmus and ambulation(*47*). When patients were tested for their ability to navigate a standardized obstacle course before administration of AAV2-hRPE65v2, 11 of 12 had great difficulty, particularly in dim light. After injection, subjects (especially children) had substantial improvement in their ambulation (Videos 1-6 below) when using their injected eye only. All LCA2 patients had bilaterally diminished full-field light sensitivity and pupillary light reflexes at baseline and they all showed improvement of at least a 2 log unit increase in pupillary light responses after GT in their treated eye. In fact, one subject had nearly the same level of light sensitivity as that in age-matched normal controls(*47*).

The success rate for recovery and magnitude of improvement was related to the age at treatment, with best results obtained in children. Visual improvement was also observed due to expansion of the visual field of the injected eye.

From the ten participants in neuroimaging study, two patients received the low dose ($1.5x10^{10}$ vector genomes), three had the medium dose ($4.8x10^{10}$ vector genomes) and five were injected with the high dose ($1.5x10^{11}$ vector genomes) of the AAV2.hRPE65v2 virus(*47*). Nine out of ten patients received their subretinal injections to their right eye and one to the left eye. All injections were administered primarily into the superior temporal aspect of their macula(*47*). This is important because the specific site in the retina chosen for vector delivery can play a key role in understanding the subsequent effects that retinal GT may have in particular locations of the visual pathway.

Informed consent (or parental permission and child assent) was obtained from all subjects for the IRB-approved GT clinical trial. These individuals were consented separately for the neuroimaging study, as were control subjects. All patients were clinically assessed as part of their qualification to enter the clinical trial for retinal GT(*46*, *47*) All control subjects were initially screened by phone and subsequently invited to participate in the study. Subjects were excluded from the neuroimaging study if they had a positive pregnancy test; expressed claustrophobia; had a metallic implanted prosthetic or device (e.g. cardiac pacemaker) or other contraindications for MRI; had excessive metallic dental work (including braces and non-removable retainers); or were non-compliant. LCA2 subjects had to meet strict inclusion/exclusion criteria in order to be invited to participate in the GT trial(*46*, *47*). None of the subjects had a history of drug/alcohol abuse. All individuals that were recruited had very close family support and provided extensive history including prescription drugs, over-the-counter medications, and food/drink habits. While there was no formal psychiatric screening carried out, each individual was interviewed in depth by several members of the study team to determine whether they could comply with the heavy time commitment and whether they had the concentration necessary to carry out all of the testing at baseline and follow-up visits.

Vision Testing and Ocular Examination

Multiple age-adapted tests of visual function were performed as part of the approved clinical trial protocol, including evaluation of visual acuity, visual field, pupillometry, and light sensitivity testing (dark adaptometry)(*46*). In addition, amplitude and frequency of nystagmus was evaluated independently for the left and right eyes.

Magnetic Resonance Imaging

MRI scans were conducted at CHOP on a research dedicated 3T Siemens Verio system using a 32-channel head coil. All scans were carried out by a single operator and monitored to be free of artifacts at the time of acquisition.

Structural Imaging

3D T1 Weighted (MPRAGE) Imaging: A 3D isotropic structural high resolution T1 sequence was acquired with inversion preparation pulse (IR-Prep: TR = 2080 ms, TE = 2.54 ms, BW =180 Hz/Px, matrix size = 320x320, FOV = 256x256 mm2, 192 axial slices, slice thickness = 0.8 mm, inversion time = 1200 ms with Flip Angle =8°, NEX = 1, Echo Spacing= 7.8, iPAT = 2 and scan

time = 7:04 minutes). This sequence was obtained for visual activation localization and the generation of group-averaged inflated hemispheres (www.brainvoyager.com).

Diffusion Tensor Imaging (DTI): The DTI sequence employed in the present study was a hybrid between the standard bipolar scheme, a monopolar Stejskal-Tanner implementation, and a modification of the latter (Siemens Medical Systems). The sequence was used with a total of 30 non-parallel diffusion gradient directions and a diffusion sensitization b-factor of 1000 s/mm^2 and four b0 images for the acquisition of 80 contiguous isotropic (1.7 x 1.7 x 1.7 mm^3) slices through the whole brain with no gaps. Sequence parameters for diffusion tensor imaging were: TR = 1100 ms, TE = 76 ms, matrix size = 128 x 128, FOV = 220x220 mm^2, bandwidth of 1446 Hz/Px, number of excitation NEX = 1 and acceleration factor (iPAT)=2 with a total acquisition time of 7:14 minutes.

DTI Voxel-Based Analysis (VBA): Prior to VBA analysis, diffusion tensor volumes were spatially normalized using PipeDream (http://brianavants.wordpress.com/software/). The normalized tensor volumes were then used to compute scalar images for fractional anisotropy (FA), radial diffusivity (RD) ($\lambda_{\perp}= (\lambda_2+\lambda_3)/2$), axial diffusivity (AD) ($\lambda_{||} =\lambda_1$), and mean diffusivity (MD) [$D=(\lambda_1+\lambda_2+\lambda_3)/3$](*48*). The normalized scalar images were smoothed with a 6 mm Gaussian kernel (in 3D). To limit the analysis to primarily white matter brain areas, a conservative white matter mask was computed to exclude cortical and subcortical gray matter and CSF. The mask was constructed by averaging the normalized FA images of all subjects and subsequently thresholded to retain only the major white matter bundles. The same mask was used for the VBA analysis. Statistical analyses were performed using the MRIcron software (http://www.mccauslandcenter.sc.edu/mricro/), which uses a permuted Brunner–Munzel (BM) rank order statistic(*49*). Brunner-Munzel(*50*) is also known as the Generalized Wilcoxon Test and is more appropriate than the t-test for data that is not normally distributed. Diffusion data in the current study did not follow a normal distribution, thus BM was used for all data analyses. Comparisons were conducted across all the voxels in the entire brain volume. To correct for multiple comparisons, we used the false discovery rate (FDR) and a corrected (alpha) level of $q < 0.05$. As an additional safeguard against false positives, we only retained clusters of size greater than 100 voxels for all analyses. To provide a common reference for our findings, we have further registered the population-based template, and thresholded FA, RD, and AD images to the MNI template to report the locations of the significant clusters in the MNI coordinates along with their MNI reported Brodmann areas (BA) (http://noodle.med.yale.edu/~papad/mni2tal/).

Diffusion Tensor Tractography: Tractography was performed on a population-based diffusion tensor template constructed from diffusion tensor images of LCA2 patients and matched controls using DTI-TK(*51*, *52*). We used a different technique of registration (DTI-TK) from the VBA analyses (PipeDream) to maximize the independence of the tractography results. Specific fibers of interest were extracted from the diffusion tensor template using DTIStudio, which is a program based on the *fiber assignment by continuous tracking* (FACT) method(*53*). Fibers were selected by initiating a seed pixel in the anatomy of choice using the “OR” operation function of DTIStudio. From this seed point a line is propagated which follows the principal eigenvector in 3D contiguous space from voxel to voxel(*53*). A threshold of 0.15- 0.20 for FA value(*53*) and a turning angle of 41°(*54*, *55*) were used. A subset of projections that were not part of the tracts of

interest were excluded using the “NOT” operation in DTIStudio. Major fiber tracts connecting to the visual cortex or forming a part of the visual pathway, such as bilateral optic radiations, inferior longitudinal fasciculus (ILF), inferior fronto-occipital fasciculus (IFO), optic chiasm, occipito-callosal (OC) and geniculostriate (GS) fibers as well as a set of control fibers that are not related to vision such as corticospinal tracts (CST), were extracted to examine whether regaining sight, due to GT, would have an effect on the major fiber tracts. After extraction, the tract-specific fibers were superimposed as an anatomical ROI onto the normalized FA images for each subject in order to obtain the average FA of each tract for individual subjects in both LCA2 and control groups.

Functional Imaging

fMRI Sequence: Functional data were acquired using blood oxygenation level-dependent (BOLD) imaging, acquiring 3 mm isotropic resolution (matrix, 64 × 64; TR/TE, 3,000/30 ms) with a total acquisition time of 4:39 min. To permit T1 saturation, three additional volumes were acquired at the beginning of the fMRI experiment, but were not used in image analysis. A transistor-transistor logic (TTL) pulse was used to automatically start the stimuli in sync with the start of fMRI acquisition. An MRI compatible response device (a button that the subject pushed when recognizing the stimulus) was used to record subject responses. Subjects were instructed to press the button once as soon as they noticed the appearance of the checkerboard.

fMRI Paradigm*:* In the past, using simple contrast reversing checkerboard stimuli, we previously demonstrated efficacy of GT in this patient population(*1*, *34*), Similar to our earlier study, the fMRI paradigm consisted of 15-second blocks of flickering (8-Hz) black and white checkerboards which consisted of three contrasts of high, medium, and low, interleaved with 15 seconds of blank (black) screens(*1*, *34*). Subjects were asked to fixate on a yellow cross in the center of the checkerboard patterns, or, if they could not see the cross, were asked to look straight ahead. Resonance Technology VisuaStim (www.mrivideo.com) goggles featuring a digital display and a 30° horizontal field of view was used to present the fMRI stimuli. The visual paradigm was programmed in E-Prime (http://www.pstnet.com/eprime.cfm)

Real Time fMRI: The research MR system at CHOP is equipped with fMRI software that allows real time monitoring of the patients’ performance during fMRI experiments as well as their translational and rotational head motions(*56*). Using the real time feature, fMRI acquisition with ≥0.6 mm translational or ≥0.6 degrees for rotational movement was terminated, the subject informed to stay still, and the experiment restarted.

fMRI Preprocessing: All functional data from individual subjects and group averaged results were processed using BrainVoyager- QX (www.brainvoyager.com). Pre-processing of data included slice scan time correction, 3D motion correction, spatial smoothing, and temporal filtering. Sinc interpolation was used for scan time correction to ensure that all voxels in the volume represented the signal simultaneously. A high-pass temporal filter of 2 cycles/run was applied to remove signal drift. Spatial smoothing was performed using a 3 mm full-width at half-maximum (FWHM) Gaussian filter. In addition to real time monitoring of the subjects’ motions, all functional data sets were additionally processed using the motion correction algorithm implemented in BrainVoyagerQX that calculates head translation (in millimeters) and rotation (in

degree) for each volume in relation to the first volume, in order to rule out excessive motion. Since the subjects' motions were monitored at the time of data acquisition, using real time fMRI, none of the subjects showed excessive motion based on offline analyses (≥0.6 mm). Statistical analyses were performed using the general linear model (GLM) as implicated in BrainVoyagerQX. Each condition was analyzed by specifying a design matrix defined as blocks with checkerboard presentation versus blocks with blank black screen, followed by application of the hemodynamic response function and correction for multiple comparisons using the false discovery rate (fdr). Since the LCA2 subjects demonstrated the largest response to the high contrast condition(*1*, *34*), only the fMRI results from the high contrast stimuli (high contrast – rest) are correlated to the diffusion tractography results.

References:

1. M. Ashtari, L. L. Cyckowski, J. F. Monroe, K. A. Marshall, D. C. Chung, A. Auricchio, F. Simonelli, B. P. Leroy, A. M. Maguire, K. S. Shindler, J. Bennett, The human visual cortex responds to gene therapy-mediated recovery of retinal function. *J Clin Invest* **121**, 2160-2168 (2011).
2. J. H. Steiger, Tests for Comparing Elements of a Correlation Matrix. *Psychological Bulletin* **87**, 245-251 (1980).
3. R. F. Dougherty, M. Ben-Shachar, R. Bammer, A. A. Brewer, B. A. Wandell, Functional organization of human occipital-callosal fiber tracts. *Proc Natl Acad Sci U S A* **102**, 7350-7355 (2005).
4. N. Sadato, A. Pascual-Leone, J. Grafman, V. Ibanez, M. P. Deiber, G. Dold, M. Hallett, Activation of the primary visual cortex by Braille reading in blind subjects. *Nature* **380**, 526-528 (1996).
5. H. Burton, A. Z. Snyder, J. B. Diamond, M. E. Raichle, Adaptive changes in early and late blind: a FMRI study of verb generation to heard nouns. *Journal of neurophysiology* **88**, 3359-3371 (2002).
6. I. Fine, A. R. Wade, A. A. Brewer, M. G. May, D. F. Goodman, G. M. Boynton, B. A. Wandell, D. I. MacLeod, Long-term deprivation affects visual perception and cortex. *Nature neuroscience* **6**, 915-916 (2003).
7. A. Valvo, L. L. Clark, Z. S. Jastrzembska, *Sight Restoration After Long Term Blindness: The Problems and Behavior Patterns of Visual Rehabilitation*. (American Foundation for the Blind, 1971).
8. F. Valverde, Apical dendritic spines of the visual cortex and light deprivation in the mouse. *Experimental brain research* **3**, 337-352 (1967).
9. S. Borges, M. Berry, The effects of dark rearing on the development of the visual cortex of the rat. *J Comp Neurol* **180**, 277-300 (1978).
10. D. H. Hubel, T. N. Wiesel, Receptive fields, binocular interaction and functional architecture in the cat's visual cortex. *J Physiol* **160**, 106-154 (1962).
11. A. Antonini, M. P. Stryker, Development of individual geniculocortical arbors in cat striate cortex and effects of binocular impulse blockade. *J Neurosci* **13**, 3549-3573 (1993).
12. A. Antonini, M. Fagiolini, M. P. Stryker, Anatomical correlates of functional plasticity in mouse visual cortex. *J Neurosci* **19**, 4388-4406 (1999).

13. H. Yu, A. K. Majewska, M. Sur, Rapid experience-dependent plasticity of synapse function and structure in ferret visual cortex in vivo. *Proc Natl Acad Sci U S A* **108**, 21235-21240 (2011).
14. T. N. Wiesel, D. H. Hubel, Single-Cell Responses in Striate Cortex of Kittens Deprived of Vision in One Eye. *Journal of neurophysiology* **26**, 1003-1017 (1963).
15. J. S. Shimony, H. Burton, A. A. Epstein, D. G. McLaren, S. W. Sun, A. Z. Snyder, Diffusion tensor imaging reveals white matter reorganization in early blind humans. *Cerebral cortex* **16**, 1653-1661 (2006).
16. C. Yu, N. Shu, J. Li, W. Qin, T. Jiang, K. Li, Plasticity of the corticospinal tract in early blindness revealed by quantitative analysis of fractional anisotropy based on diffusion tensor tractography. *Neuroimage* **36**, 411-417 (2007).
17. N. Lepore, P. Voss, F. Lepore, Y. Y. Chou, M. Fortin, F. Gougoux, A. D. Lee, C. Brun, M. Lassonde, S. K. Madsen, A. W. Toga, P. M. Thompson, Brain structure changes visualized in early- and late-onset blind subjects. *Neuroimage* **49**, 134-140 (2010).
18. M. R. Dursteler, L. J. Garey, J. A. Movshon, Reversal of the morphological effects of monocular deprivation in the kittens's lateral geniculate nucleus. *J Physiol* **261**, 189-210 (1976).
19. S. LeVay, T. N. Wiesel, D. H. Hubel, The development of ocular dominance columns in normal and visually deprived monkeys. *J Comp Neurol* **191**, 1-51 (1980).
20. N. V. Swindale, F. Vital-Durand, C. Blakemore, Recovery from monocular deprivation in the monkey. III. Reversal of anatomical effects in the visual cortex. *Proceedings of the Royal Society of London. Series B, Containing papers of a Biological character. Royal Society* **213**, 435-450 (1981).
21. J. A. Movshon, Reversal of the physiological effects of monocular deprivation in the kitten's visual cortex. *J Physiol* **261**, 125-174 (1976).
22. S. K. Song, J. Yoshino, T. Q. Le, S. J. Lin, S. W. Sun, A. H. Cross, R. C. Armstrong, Demyelination increases radial diffusivity in corpus callosum of mouse brain. *Neuroimage* **26**, 132-140 (2005).
23. J. M. Tyszka, C. Readhead, E. L. Bearer, R. G. Pautler, R. E. Jacobs, Statistical diffusion tensor histology reveals regional dysmyelination effects in the shiverer mouse mutant. *Neuroimage* **29**, 1058-1065 (2006).
24. N. Shu, Y. Liu, J. Li, Y. Li, C. Yu, T. Jiang, Altered anatomical network in early blindness revealed by diffusion tensor tractography. *PloS one* **4**, e7228 (2009).
25. U. Noppeney, K. J. Friston, J. Ashburner, R. Frackowiak, C. J. Price, Early visual deprivation induces structural plasticity in gray and white matter. *Current biology : CB* **15**, R488-490 (2005).
26. M. Ptito, F. C. Schneider, O. B. Paulson, R. Kupers, Alterations of the visual pathways in congenital blindness. *Experimental brain research* **187**, 41-49 (2008).
27. L. A. Yannuzzi, Central serous chorioretinopathy: a personal perspective. *Am J Ophthalmol* **149**, 361-363 (2010).
28. D. C. Chung, E. I. Traboulsi, Leber congenital amaurosis: clinical correlations with genotypes, gene therapy trials update, and future directions. *Journal of AAPOS : the official publication of the American Association for Pediatric Ophthalmology and Strabismus / American Association for Pediatric Ophthalmology and Strabismus* **13**, 587-592 (2009).

29. I. Perrault, J. M. Rozet, S. Gerber, I. Ghazi, C. Leowski, D. Ducroq, E. Souied, J. L. Dufier, A. Munnich, J. Kaplan, Leber congenital amaurosis. *Molecular genetics and metabolism* **68**, 200-208 (1999).
30. K. Al-Khayer, S. Hagstrom, G. Pauer, H. Zegarra, J. Sears, E. I. Traboulsi, Thirty-year follow-up of a patient with leber congenital amaurosis and novel RPE65 mutations. *Am J Ophthalmol* **137**, 375-377 (2004).
31. D. H. Salat, E. E. Smith, D. S. Tuch, T. Benner, V. Pappu, K. M. Schwab, M. E. Gurol, H. D. Rosas, J. Rosand, S. M. Greenberg, White matter alterations in cerebral amyloid angiopathy measured by diffusion tensor imaging. *Stroke; a journal of cerebral circulation* **37**, 1759-1764 (2006).
32. C. Davatzikos, S. M. Resnick, Degenerative age changes in white matter connectivity visualized in vivo using magnetic resonance imaging. *Cerebral cortex* **12**, 767-771 (2002).
33. P. Kochunov, D. E. Williamson, J. Lancaster, P. Fox, J. Cornell, J. Blangero, D. C. Glahn, Fractional anisotropy of water diffusion in cerebral white matter across the lifespan. *Neurobiol Aging* **33**, 9-20 (2012).
34. J. Bennett, M. Ashtari, J. Wellman, K. A. Marshall, L. L. Cyckowski, D. C. Chung, S. McCague, E. A. Pierce, Y. Chen, J. L. Bennicelli, X. Zhu, G. S. Ying, J. Sun, J. F. Wright, A. Auricchio, F. Simonelli, K. S. Shindler, F. Mingozzi, K. A. High, A. M. Maguire, AAV2 gene therapy readministration in three adults with congenital blindness. *Sci Transl Med* **4**, 120ra115 (2012).
35. R. W. Hertle, L. F. Dell'Osso, *Nystagmus in Infancy and Childhood: Current Concepts in Mechanisms, Diagnoses, and Management*. (Oxford University Press, 2013).
36. D. H. Hubel, T. N. Wiesel, The period of susceptibility to the physiological effects of unilateral eye closure in kittens. *J Physiol* **206**, 419-436 (1970).
37. W. J. Pan, G. Wu, C. X. Li, F. Lin, J. Sun, H. Lei, Progressive atrophy in the optic pathway and visual cortex of early blind Chinese adults: A voxel-based morphometry magnetic resonance imaging study. *Neuroimage* **37**, 212-220 (2007).
38. D. A. Paul, E. Gaffin-Cahn, E. B. Hintz, G. J. Adeclat, T. Zhu, Z. R. Williams, G. E. Vates, B. Z. Mahon, White matter changes linked to visual recovery after nerve decompression. *Sci Transl Med* **6**, 266ra173 (2014).
39. R. D. Fields, White matter in learning, cognition and psychiatric disorders. *Trends Neurosci* **31**, 361-370 (2008).
40. T. Ishibashi, K. A. Dakin, B. Stevens, P. R. Lee, S. V. Kozlov, C. L. Stewart, R. D. Fields, Astrocytes promote myelination in response to electrical impulses. *Neuron* **49**, 823-832 (2006).
41. Y. Kozorovitskiy, C. G. Gross, C. Kopil, L. Battaglia, M. McBreen, A. M. Stranahan, E. Gould, Experience induces structural and biochemical changes in the adult primate brain. *Proceedings of the National Academy of Sciences of the United States of America* **102**, 17478-17482 (2005).
42. S. L. Bengtsson, Z. Nagy, S. Skare, L. Forsman, H. Forssberg, F. Ullen, Extensive piano practicing has regionally specific effects on white matter development. *Nature neuroscience* **8**, 1148-1150 (2005).
43. J. Scholz, M. C. Klein, T. E. Behrens, H. Johansen-Berg, Training induces changes in white-matter architecture. *Nature neuroscience* **12**, 1370-1371 (2009).

44. M. Taubert, B. Draganski, A. Anwander, K. Muller, A. Horstmann, A. Villringer, P. Ragert, Dynamic properties of human brain structure: learning-related changes in cortical areas and associated fiber connections. *J Neurosci* **30**, 11670-11677 (2010).
45. E. M. Stone, Leber congenital amaurosis - a model for efficient genetic testing of heterogeneous disorders: LXIV Edward Jackson Memorial Lecture. *Am J Ophthalmol* **144**, 791-811 (2007).
46. A. M. Maguire, F. Simonelli, E. A. Pierce, E. N. Pugh, Jr., F. Mingozzi, J. Bennicelli, S. Banfi, K. A. Marshall, F. Testa, E. M. Surace, S. Rossi, A. Lyubarsky, V. R. Arruda, B. Konkle, E. Stone, J. Sun, J. Jacobs, L. Dell'Osso, R. Hertle, J. X. Ma, T. M. Redmond, X. Zhu, B. Hauck, O. Zelenaia, K. S. Shindler, M. G. Maguire, J. F. Wright, N. J. Volpe, J. W. McDonnell, A. Auricchio, K. A. High, J. Bennett, Safety and efficacy of gene transfer for Leber's congenital amaurosis. *The New England journal of medicine* **358**, 2240-2248 (2008).
47. A. M. Maguire, K. A. High, A. Auricchio, J. F. Wright, E. A. Pierce, F. Testa, F. Mingozzi, J. L. Bennicelli, G. S. Ying, S. Rossi, A. Fulton, K. A. Marshall, S. Banfi, D. C. Chung, J. I. Morgan, B. Hauck, O. Zelenaia, X. Zhu, L. Raffini, F. Coppieters, E. De Baere, K. S. Shindler, N. J. Volpe, E. M. Surace, C. Acerra, A. Lyubarsky, T. M. Redmond, E. Stone, J. Sun, J. W. McDonnell, B. P. Leroy, F. Simonelli, J. Bennett, Age-dependent effects of RPE65 gene therapy for Leber's congenital amaurosis: a phase 1 dose-escalation trial. *Lancet* **374**, 1597-1605 (2009).
48. C. Pierpaoli, P. J. Basser, Toward a quantitative assessment of diffusion anisotropy. *Magn Reson Med* **36**, 893-906 (1996).
49. T. E. Nichols, A. P. Holmes, N
onparametric permutation tests for functional neuroimaging: a primer with examples. *Hum Brain Mapp* **15**, 1-25 (2002).
50. E. Brunner, U. Munzel, The Nonparametric Behrens-Fisher Problem: Asymptotic Theory and a Small-Sample Approximation. *Biometrical Journal* **42**, 17-25 (2000).
51. H. Zhang, P. A. Yushkevich, D. C. Alexander, J. C. Gee, Deformable registration of diffusion tensor MR images with explicit orientation optimization. *Med Image Anal* **10**, 764-785 (2006).
52. H. Zhang, P. A. Yushkevich, D. Rueckert, J. C. Gee, Unbiased white matter atlas construction using diffusion tensor images. *Medical image computing and computer-assisted intervention : MICCAI ... International Conference on Medical Image Computing and Computer-Assisted Intervention* **10**, 211-218 (2007).
53. S. Mori, W. E. Kaufmann, C. Davatzikos, B. Stieltjes, L. Amodei, K. Fredericksen, G. D. Pearlson, E. R. Melhem, M. Solaiyappan, G. V. Raymond, H. W. Moser, P. C. van Zijl, Imaging cortical association tracts in the human brain using diffusion-tensor-based axonal tracking. *Magn Reson Med* **47**, 215-223 (2002).
54. T. Okada, Y. Miki, Y. Fushimi, T. Hanakawa, M. Kanagaki, A. Yamamoto, S. Urayama, H. Fukuyama, M. Hiraoka, K. Togashi, Diffusion-tensor fiber tractography: intraindividual comparison of 3.0-T and 1.5-T MR imaging. *Radiology* **238**, 668-678 (2006).
55. S. Wakana, H. Jiang, L. M. Nagae-Poetscher, P. C. van Zijl, S. Mori, Fiber tract-based atlas of human white matter anatomy. *Radiology* **230**, 77-87 (2004).
56. M. Ashtari, L. Cyckowski, A. Yazdi, A. Viands, K. Marshall, I. Bókkon, A. Maguire, J. Bennett, fMRI of Retina-Originated Phosphenes Experienced by Patients with Leber Congenital Amaurosis. *PloS one* **9**, e86068 (2014).

Videos:

1. *http://www.thelancet.com/cms/attachment/2001002122/2003731820/mmc4.mpg*
2. *www.thelancet.com/cms/attachment/2001002122/2003731821/mmc5.mpg*
3. *http://www.thelancet.com/cms/attachment/2001002122/2003731822/mmc6.mpg*
4. *www.thelancet.com/cms/attachment/2001002122/2003731823/mmc7.mpg*
5. *http://www.thelancet.com/cms/attachment/2001002122/2003731818/mmc2.mpg*
6. *http://www.thelancet.com/cms/attachment/2001002122/2003731819/mmc3.mpg*

Acknowledgements

We are grateful for funding provided by the R21EY020662, Foundation Fighting Blindness (FFB)–sponsored CHOP-PENN Pediatric Center for Retinal Degenerations, C-GT-0913-06280UPA03, 8DP1EY023177, 1R24EY019861, TAPITMAT grants, Research to Prevent Blindness (RPB), and the F.M. Kirby Foundation. CIB is supported by the Intramural Research Program of NIMH. We thank Dr. Thorsten Feirweier of Siemens for providing us with the diffusion sequence. We also thank Jamie Rundio, Peter Lam, Rachel Golembski, and John Dell for their expert technical assistance.